Acta Neuropathol (2009) 117:457–464
DOI 10.1007/s00401-008-0467-y

CASE REPORT

Novel genomic amplification targeting the microRNA cluster at 19q13.42 in a pediatric embryonal tumor with abundant neuropil and true rosettes

Stefan Pfister · Marc Remke · Mirco Castoldi · Alfa H. C. Bai · Martina U. Muckenthaler · Andreas Kulozik · Andreas von Deimling · Armin Pscherer · Peter Lichter · Andrey Korshunov

Received: 23 October 2008 / Revised: 24 November 2008 / Accepted: 24 November 2008 / Published online: 5 December 2008

Abstract Embryonal tumors with abundant neuropil and true rosettes (ETANTR) comprise a rare variant of embryonal brain tumors usually occurring in infants. Only 13 cases have been reported in the literature to date and little is known about the molecular pathogenesis of these tumors. Here, we describe a case of ETANTR in a 2-year-old girl presenting with a large tumor in the vermis of the cerebellum. Histological examination showed clusters of small-undifferentiated cells including ependymoblastic-like rosettes admixed with large fibrillar and paucicellular neuropil-like areas indicative for ETANTR. Genomic imbalances were detected by using array-based comparative genomic hybridization. In addition to trisomy of chromosome 2, which has been previously described in ETANTR, array-CGH revealed high-level genomic amplification of 0.89 Mb at chromosome band 19q13.42 covering a microRNA cluster and several protein-coding genes. This aberration has not been described in any other brain tumor to date, indicating a specific aberration in ETANTR. MicroRNAs contained in the microRNA cluster at 19q13.42 including oncomirs miRNA-372 and miRNA-373 were highly up-regulated in the tumor when compared to normal cerebellum or whole brain. In summary, this is the first report on a potentially specific genetic aberration in ETANTR, supporting the hypothesis of a distinct tumor entity.

Electronic supplementary material The online version of this article (doi:10.1007/s00401-008-0467-y) contains supplementary material, which is available to authorized users.

S. Pfister (✉) · M. Remke · A. H. C. Bai · A. Pscherer · P. Lichter
Division Molecular Genetics, German Cancer Research Center,
Im Neuenheimer Feld 280, 69120 Heidelberg, Germany
e-mail: s.pfister@dkfz.de

S. Pfister · M. Castoldi · M. U. Muckenthaler · A. Kulozik
Department of Pediatric Oncology, Hematology and Immunology,
University of Heidelberg, Im Neuenheimer Feld 430,
Heidelberg, Germany

M. Castoldi
Gene Expression Programme,
European Molecular Biology Laboratory,
Meyerhofstrasse 1, 69117 Heidelberg, Germany

A. von Deimling · A. Korshunov
Department of Neuropathology, University of Heidelberg,
Im Neuenheimer Feld 220/221, 69120 Heidelberg, Germany

A. von Deimling · A. Korshunov
Clinical Cooperation Unit Neuropathology,
German Cancer Research Center,
Im Neuenheimer Feld 280, 69120 Heidelberg, Germany

Introduction

Embryonal tumors represent the largest group of malignant brain tumors in childhood. The 2007 WHO classification of central nervous system tumors recognizes three main histological entities all of which contain a population of primitive ("embryonal") cells, i.e., medulloblastoma, atypical teratoid/rhabdoid tumor, and CNS primitive neuroectodermal tumors (PNETs) [8]. In addition, the latter entity is subdivided into CNS neuroblastoma/ganglioneuroblastoma, medulloepithelioma, and ependymoblastoma. Recently, a yet different pediatric embryonal brain tumor has been described by Eberhart and co-workers that occupies an intermediate position between CNS neuroblastoma and ependymoblastoma [4]. Based on its characteristic histopathological findings, this tumor was designated "embryonal tumor with abundant neuropil and true rosettes (ETANTR)". This tumor entity shows a unique combination of histological,

immunohistochemical and ultrastructural features. To date, only 13 cases of these tumors have been reported [3–6]. All patients were very young children (range from 1 to 4 years). In contrast, there were no correlations with regard to gender and tumor localization with tumors occurring in cerebral hemispheres, cerebellum, and brain stem.

Discussions are proceeding on whether these tumors represent a distinct entity or only a variation of parent PNETs. Molecular analysis by fluorescence in situ hybridization (FISH) was only performed in three cases and two of them showed abnormalities of chromosome 17. Therefore, molecular similarity of these tumors to medulloblastoma has been suggested. In the present study, we performed array-CGH analysis and microRNA (miRNA) screening of one ETANTR and identified a novel high-level amplification within chromosomal region 19q13.42 containing a cluster of miRNA coding genes. This finding has not been detected in any other pediatric brain tumor studied with the same array-CGH platform to date (approximately 200 cases), which allows us to hypothesize a unique nosologic position of ETANTR.

Materials and methods

Case report

A 2-year-old girl presented with a 1-month history of personality changes and ataxia. Morning headache, nausea and vomiting appeared 2 weeks before admission to the Burdenko Neurosurgical Institute, Moscow, Russia. In addition, her parents noted appearance of divergent strabism. Neurological examination disclosed ataxia, tetraparesis and central right seventh cranial nerve palsy.

CT and MRI scans with contrast enhancement revealed a homogeneous and poorly contrasted tumor mass located in the middle and upper parts of the vermis cerebelli with protrusion into the cavity of the fourth ventricle. The upper part of the tumor also spread into the pineal region through the tentorial incisure. Occlusive hydrocephalus with dilatation of the third and both lateral ventricles was obvious at presentation. Spinal MRI and CSF cytological analysis at admission were negative.

Subtotal resection of the tumor could be achieved by open neurosurgery. Postoperative MRI disclosed a tumor residue near the tentorium cerebelli, and the large cerebral vein (Galeni) was included in the residual tumor. Postsurgical course was uneventful and some improvement in patient's neurological status was noted. The child was then treated with high-dose chemotherapy (including stem cell rescue) and thereafter she received local radiotherapy for a total dose of 56 Gy to the tumor bed. Finally, she received six courses of maintenance chemotherapy consisting of cisplatin, lomustine and vincristin. Eighteen months after subtotal tumor resection, the patient is alive and craniospinal MRI performed 17 months after the operation showed no evidence of tumor re-growth with a stable size of the tumor remnants.

Immunohistochemistry

For immunohistochemical analysis, a panel of antibodies directed against the following antigens was applied: glial fibrillary acidic protein (GFAP) (6F2; 1:200: DAKO); synaptophysin (polyclonal; RTU; DAKO); neurofilament protein (2F11; RTU; DAKO); smooth muscle actin (1A4; RTU; DAKO), vimentin (V9; RTU; DAKO); EMA (E29; RTU; DAKO); cytokeratin (AE1/AE3; RTU; DAKO); cytokeratin CAM 5.2 (5D3; 1:50; BioGenex), CD99 (12E7; RTU; DAKO); NeuN (MAB 377; 1:1000;Chemicon); BAF47/INI1 (BAF47; 1:80; BD Biosciences); Ki-67 (SP-6; 1:200; NeoMarkers). For antigen retrieval, the sections were microwaved in antigen unmask solution (BD Bioscience San Jose, CA, USA). Immunostaining was visualized by means of the DAKO Envision system using diaminobenzidine as a chromogen.

Nucleic acid isolation

Extraction of high-molecular-weight DNA and total RNA from frozen tumor samples was carried out by use of cesium chloride ultracentrifugation [13]. Genomic DNA from peripheral blood mononuclear cells of healthy donors (pool of ten donors, age 25–40 years for each gender) was isolated by use of the Qiagen DNA Blood Midi-Kit (Hilden, Germany).

Array-based comparative genomic hybridization (array-CGH)

Array-CGH (matrix-CGH) [12] was carried out as previously described [9, 15]. Selection of genomic clones, isolation of BAC DNA, performance of DOP-PCR, preparation of microarrays, labeling, hybridization, and washing procedures were performed as outlined.

Microarray data analysis

Raw data processing and normalization was performed as previously reported [9] providing $\log_2$-ratios of spot intensities. The chromosomal mapping information is based on the University of California at Santa Cruz (UCSC) genome database (March 2006) and the March 2006 (hg18) assembly (NCBI Build 36.1) of the International Human Genome Sequencing Consortium.

Fluorescence in situ hybridization (FISH)

Two-color interphase FISH to the sections was performed using the following fluorochrome-labeled commercial probe sets (Vysis, Inc.): centromere (CEP)7/7p12(*EGFR)* dual color probe set; CEP9/9p21(*CDKN2A)* dual color probe set; CEP10/10q23(*PTEN)* dual color probe set; CEP2/2p24(*MYCN)* dual color probe set; CEP8 and locus specific 8q24(*MYC)* probe; locus-specific 17p13(*LIS1)*/ 17q21(*RARA*) dual color probe set; mixed locus-specific 1p36/1q25 and 19p13/19q13 dual color probe sets; orange-labeled 20q13(*ZNF217)* locus probe, green-labeled 22q11(*BCR)* locus probe, and subtelomere probes for 19p13.3 and 19q13.4. Pretreatment of slides, hybridization, post-hybridization processing, and signal detection were performed as previously described [1]. Signals were scored in at least 200 non-overlapping, intact nuclei. Metaphase FISH for verifying clone-mapping position was performed using peripheral blood cell cultures of healthy donors as previously outlined [7].

miCHIP analysis

Total RNA (300 ng) was labeled with a Cy3-conjugated RNA linker (Biospring, Frankfurt, Germany) and hybridized to miCHIP as previously described [13]. miCHIP is based on locked nucleic acid (LNA) technology, whereby LNA-modified, Tm-normalized miRCURY capture probes (Exiqon, Denmark) designed to target 550 unique human miRNAs (miRbase v9.2, Wellcome Trust Sanger Institute, http://microrna.sanger.ac.uk/) were printed onto Codelink slides (GE Healthcare, Chalfont St Giles, UK). Array images were generated by using a Genepix 4200AL laser scanner (Molecular Devices, USA) where miCHIP arrays were scanned using the Genepix auto PMT (Photo Multiplayer) algorithm, with pixel saturation tolerance set to 0.2%. Tiff images generated by the Genepix 4200AL laser scanner were processed by the Genepix 6 microarray analysis software (Molecular Devices, USA). Artifact-associated spots were eliminated both by software- and visual-guided flags. Signal intensities were measured according to the local background subtraction method. All probes were spotted in duplicate and the median signal intensity of these was calculated. miCHIP data were median normalized for subsequent analysis and log2-ratios (tumor/control pool of normal cerebellum) were calculated.

Quantitative real-time PCR (QRT-PCR)

To measure *PRKCG1* and *TFPT* mRNA abundance in the tumor sample, a reference of total RNA obtained from normal human cerebellum of 24 individuals (age 16–70; BD Bioscience, USA) was used for tissue-specific normalization. Each cDNA sample was analyzed in triplicate with the ABI PRISM 7700 (Applied Biosystems, USA) using Absolute SYBR Green ROX Mix (ABgene, UK) according to the manufacturer's instructions. Two endogenous housekeeping genes (*PGK1*, *DCTN2*) were used as internal standards. These genes were not regulated in expression profiling experiments comparing pediatric low-grade astrocytomas and medulloblastomas. Furthermore, they were tested in normal tissues from whole brain and cerebellum in which they displayed very little variability. All primers were tested to exclude amplification from genomic DNA. The relative quantification of the RNA of interest in comparison to the housekeeping genes was calculated according to a previously published algorithm with the modification that two housekeeping genes were used in the present study [10]. Oligonucleotide sequences are available upon request.

To validate our miChip findings, QRT-PCR of selected miRNAs was performed using commercially available Taqman Kits and miRNA-specific probes from Applied Biosystems (USA). Taqman analysis was carried out according to the manufacturer's instructions. RNU66 and RNU6B were used as housekeepers. miRNA abundance in the tumor was normalized against the housekeepers and plotted against normal cerebellum (BD Bioscience, USA, as for the protein-coding genes) or whole brain (pool of donors, Biocat, Germany).

Results

Pathological examination

On light microscopical investigation, the tumor showed a biphasic pattern featuring highly cellular clusters of small cells with round or polygonal nuclei and scanty cytoplasm admixed with large fibrillar and paucicellular neuropil-like areas (Fig. 1a). Among the clusters and aggregates of small cells, numerous true ependymoblastic-like rosettes were identified (Fig. 1b). The latter were mitotically active and multilayered with well-formed central round or slit-like lumina in the absence of an outer membrane. The lumina of the rosettes were either empty or filled with eosinophilic debris. Perivascular and Homer-Wright rosettes were absent. Mitotic figures were frequently observed in highly cellular areas and in the rosettes as well as prominent apoptotic bodies. There were no microvascular proliferates and necrotic areas in this neoplasm. The combination of histopathological patterns mentioned above fulfills all diagnostic criteria of an "embryonal tumor with abundant neuropil and true rosettes" (ETANTR), as previously described by Eberhart and co-workers [4].

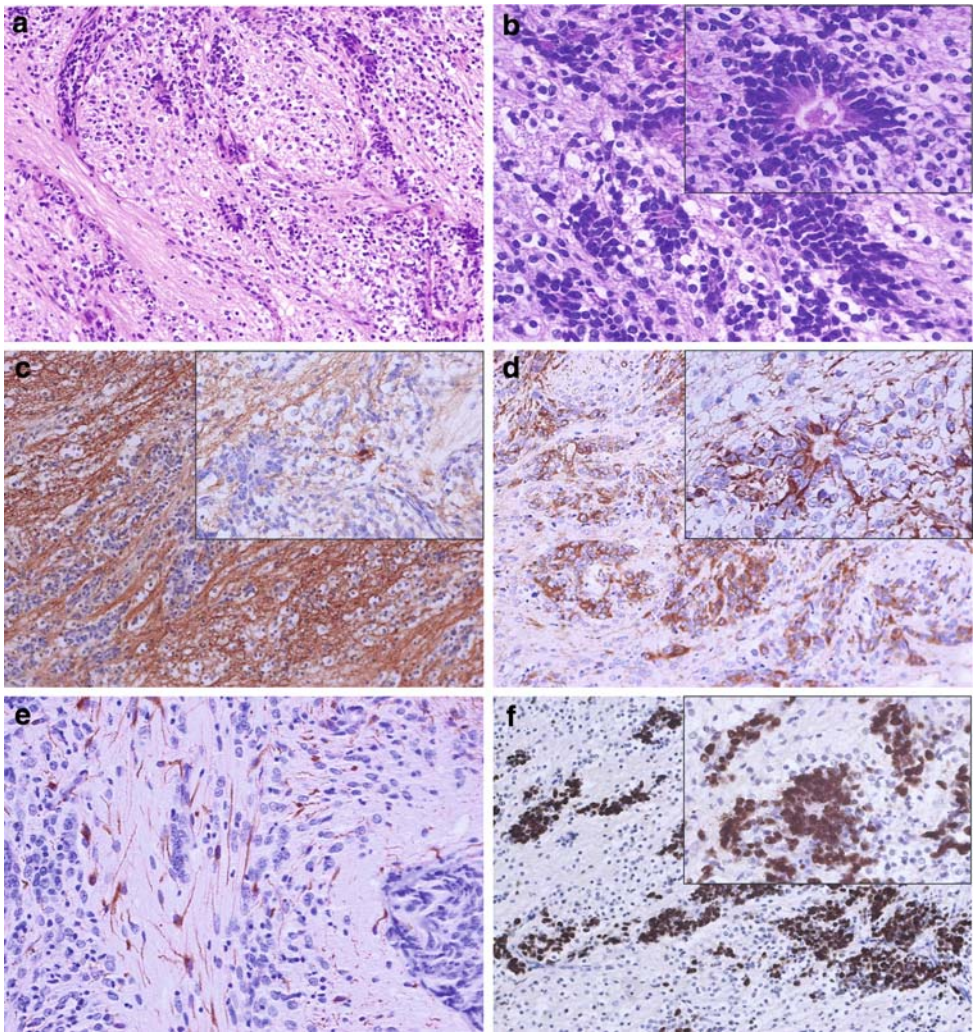

Fig. 1 Microscopic appearance and immunohistochemical patterns of the ETANTR. **a** (H&E; ×100) Neurocytic paucicellular areas with numerous rosettes embedded within abundant neuropil. **b** (H&E; ×200) Clusters of small cells and rosettes; *inset* of an ependymoblastic-like rosette (H&E; ×400). **c** Strong expression of synaptophysin in paucicellular areas and neuropil (X100); *inset* only single cells are synaptophysin-positive in cell-rich areas (×200). **d** Strong vimentin expression in cell-rich areas (×200); *inset* vimentin expression in rosette-forming cells (×400). **e** Single cells stain positive for GFAP (×200). **f** Expression of Ki-67 was predominately identified in cell-rich areas (×100); *inset* Ki-67 expression within an ependymoblastic rosette (×400)

Immunohistochemical analysis revealed strong positivity for synaptophysin within the neuropil-like tumor part, whereas only some positive cells were observed within the cell-rich tumor part (Fig. 1c). Nuclei of cells within neuropil were also positive for Neu-N antigen. Additionally, the paucicellular tumor part included single ganglioid-like cells that were highlighted upon immunostaining of neurofilament proteins. In contrast, the cell-rich part of the tumor was strongly positive for vimentin; which was also positive in the cells forming true rosettes (Fig. 1d). CD99 immunoreactivity was predominantly membranous or dot-like and was detected within the apical parts of the primitive cells forming true rosettes. Tumor cells were negative for actin, EMA and cytokeratins, whereas single entrapped astrocytes were positive for GFAP (Fig. 1e). Nuclear expression of the BAF47/INI1 protein was found in tumor nuclei throughout both components of the tumor. Ki-67 nuclear expression was found predominantly in the densely cellular areas including rosettes (Fig. 1f), and the mean Ki-67 index was 47%.

DNA-copy number aberrations

Array-based comparative genomic hybridization revealed multiple, predominantly yet unknown DNA copy number imbalances including aberrations affecting entire chromosomes, e.g., trisomy of chromosomes 2 and 19 (Fig. 2a). Most interestingly, a novel high-level genomic amplification of 0.89 Mb at chromosome band 19q13.42 was identified, which has not been described in any other human cancer to date (Fig. 2c). The amplification was found to cover a total of 29 known protein-coding genes (Supplementary Table 1). Based on their reported and putative role in cancer, amplification of the *TFPT* gene, which acts as a fusion partner of E2A in childhood ALL, and the *PRKCG* gene, a member of the protein kinase C family of genes, were of particular interest. In addition, 25 genes coding for a cluster of miRNAs at 19q13.42 were affected by this amplification (Supplementary Table 2). Regions of copy-number aberrations smaller than 3 Mb in size are listed in Table 1. Small copy-number

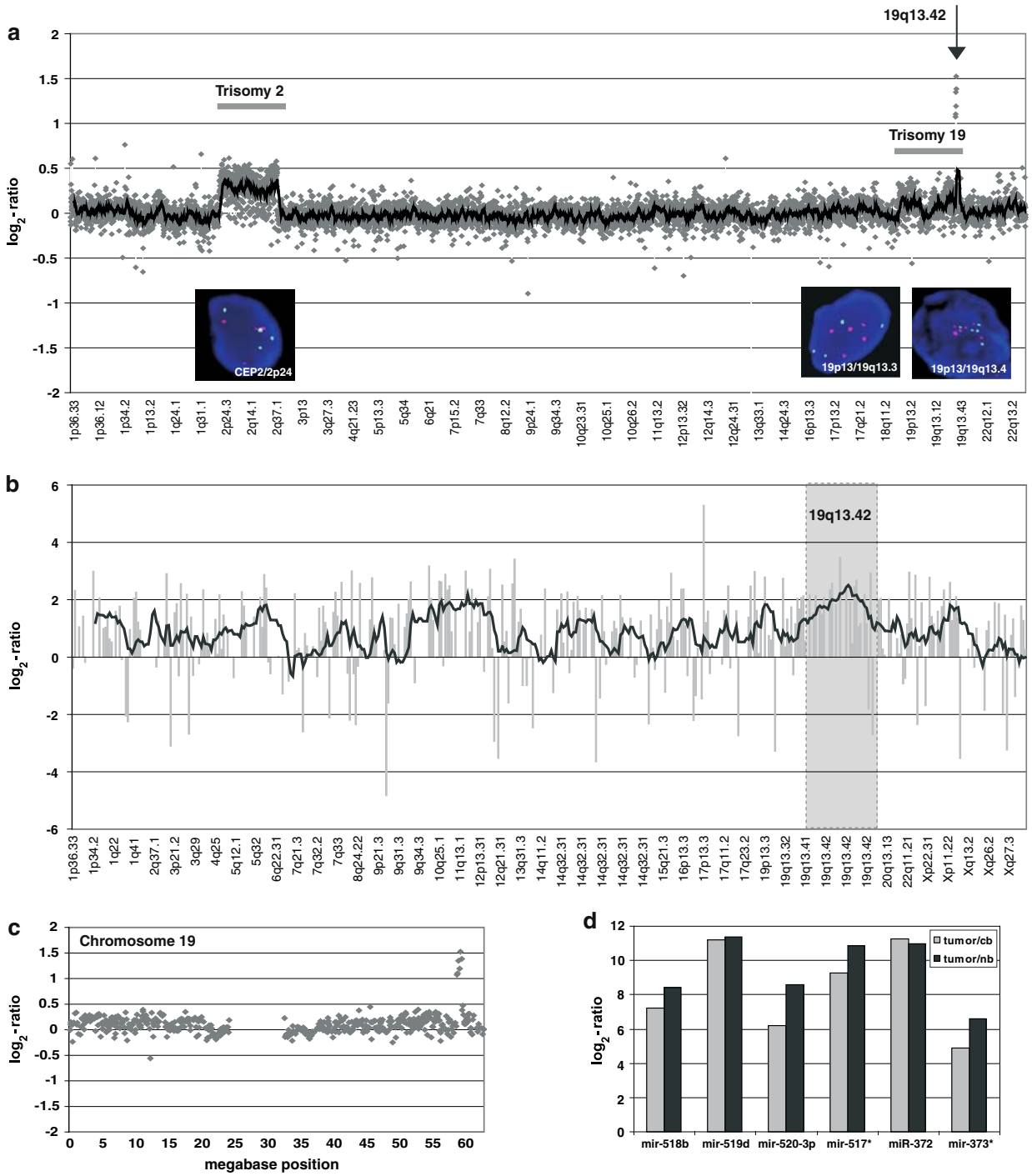

Fig. 2 Array-CGH and miRNA-expression profiling results. **a** Genome-wide array-CGH profile of the ETANTR hybridized against a pool of DNA derived from mononuclear peripheral blood cells from 10 healthy donors. Clones are plotted in order of chromosomal annotation (*x*-axis). Ratios (ETANTR/control) are given as $\log_2$-ratios (*y*-axis). Large genomic aberrations were detected on chromosomes 2 and 19 (trisomies). As indicated by an *arrow*, a high-level genomic amplification (>4 copies on average) was observed at 19q13.42. Results of large aberrations were validated by FISH analysis. Labeling of probes was as follows: CEP2 *green*/2p24 *red*, 19p13.3 *green*/19q13.3 *red*, and 19p13.3 *green*/19q13.4 *red*. **b** Genome-wide miRNA profile as obtained by comparison of miRNA expression in the ETANTR with expression in a pool of normal cerebellum (24 healthy individuals). Clones are plotted in chromosomal order (*x*-axis) and $\log_2$-ratios are given for ETANTR/control. **c** Magnification of the array-CGH profile at chromosome 19 indicating a low-level gain for the whole chromosome and a high-level amplification (>4 copies on average) at 19q13.42. **d** Expression of selected miRNAs at chromosome band 19q13.42 was validated by QRT-PCR. All tested miRNAs were highly upregulated in the tumor when compared to either normal cerebellum (*light gray bars*) or whole brain (*dark gray bars*). Expression ratios are given as $\log_2$-ratios. Normalization was performed against two housekeeping genes (*RNU66* and *RNU6B*) which showed comparable expression in all samples

Table 1 Small genomic aberrations <1 Mb in size

Localization	Type of aberration	Start clone	End clone	Size (Mb)	Candidate gene(s)
1q31.2	Loss	RP11-184O20	RP5-1116C7	0.32	DNM3
1q31.3	Loss	RP11-466M12	RP11-268N1	0.30	NA
4q24	Loss	RP11-13F20	RP11-167N19	0.45	EMCN
6p21.33	Gain	RP11-201G24	RP11-215O12	0.35	CSNK2B
10q23.31	Loss	RP11-477D14	RP11-15K3	0.24	NA
13q33.3	Loss	RP11-381O6	RP11-219B15	0.22	NA
14q22.3	Loss	RP11-132J14	RP11-484F16	0.79	PELI2; KTN1
16q21	Loss	RP11-148F12	RP11-370P15	0.14	NA
17q25.1	Gain	RP11-474I11	RP11-685I11	0.52	ACOX1; FOXJ1, CDK3
19q13.42	Amplification	CTC-339O9	CTD-2587H19	0.89	TFPT, PRKCG, miRNA cluster
22q12.3	Gain	LL22NC03-2E9	LL22NC03-13E1	0.09	LARGE1
22q13.2	Gain	RP5-1057D18	RP11-554C12	0.09	SsRNA U6; RBX1

Table 2 Clinical and molecular findings in all cases of ETANTR reported in the literature to date

No	Age	Gender	Localization	Level of resection	Adjuvant therapy	Follow-up	Genomic aberrations	References
1	2	Female	Corpus callosum/right frontal	Subtotal	Chemotherapy	DOD, 6 months	N/A	[1]
2	2.5	Male	Left frontoparietal	Subtotal	Chemotherapy; radiotherapy	DOD, 11 months	N/A	[1]
3	3.5	Male	Bifrontal	Subtotal	Chemotherapy; radiotherapy	DOD, 14 months	N/A	[1]
4	1	Female	Right frontoparietal	Subtotal	None	DOD, 11 months	N/A	[1]
5	1	Female	Tectal plate	Subtotal	Chemotherapy	DOD, 5 months	N/A	[1]
6	2	Female	Left frontal	Subtotal	HD-chemotherapy; BMT	NED, 30 months	N/A	[1]
7	3	Female	Right frontal	Subtotal	Chemotherapy	AWD, 7 months	N/A	[1]
8	1.5	Male	Cerebellum	N/A	N/A	DOD, 10 months	N/A	[1]
9	2	Female	Frontal	N/A	N/A	N/A	N/A	[1]
10	4	Male	Left parieto-occipital	Gross total	Chemotherapy; radiotherapy	DOD, 6 months	i(17q)	[2]
11	4	Male	Midbrain/pons	Subtotal	Chemotherapy; radiotherapy	AWD, 19 months	+2; +8; +17; +22	[2]
12	4	Female	Midbrain/pons	Subtotal	Chemotherapy; radiotherapy	NED, 34 months	N/A	[3]
13	2	Male	Left parieto-occipital	Near total	None	PD, 16 months	2, 8, 17 balanced	[4]
14	2	Female	Vermis cerebelli	Subtotal	HD-chemotherapy; BMT; radiotherapy	SD, 16 months	+2; +19; amp19q13.42	

HD high-dose, *BMT* bone-marrow transplantation, *DOD* death of disease, *NED* no evidence of disease, *AWD* alive with disease, *PD* progressive disease, *SD* stable disease, *N/A* not available

aberrations defined possible candidate genes known to be involved in tumorigenesis. Gains included potent oncogenes such as *CDK3*, and *FOXJ1*. Losses harbored genes involved in cell adhesion (*DNM3*, *EMCN*) among others.

Confirmation of findings by FISH

FISH analysis of selected loci confirmed a low-level gain of chromosome 2 (>10% of nuclei with more than 3 signals for both 2p24/*MYCN* and CEP2 probes), as well as chromosomal

gains of 19p and 19q identified by using both, subtelomere and locus-specific probes (Fig. 2a). Probes against chromosomes 1, 7, 8, 9 10, 17, 20q and 22q revealed normal dosages (i.e., two copies).

mRNA expression of candidate oncogenes

Messenger-RNA expression of the candidate oncogenes *TFPT* and *PRKCG1* was assessed by quantitative real-time PCR. mRNA abundance in the tumor was normalized against two housekeeping genes (*PGK1*, *DCTN2*). When compared to the reference RNA (pool of normal cerebellum from 24 donors, age 16–70 years), no significant up-regulation of these genes was detected (data not shown).

Overexpression of the miRNA cluster located at 19q13.42

To assess whether the cluster of 25 known miRNA genes at 19q13.42 might be a target of the genomic amplification, we performed a genome-wide miRNA-profiling using a LNA-based approach as previously described [2]. Interestingly, the miRNA-genes at 19q13.42 were among the most abundantly expressed miRNAs across the genome (Fig. 2b; Supplementary Table 2). Expression of selected miRNAs was validated by QRT-PCR (Fig. 2d). The function of the miRNAs showing the highest up-regulation in the chip-experiment (miRNA-518b, miRNA-519d, miRNA-520-3p, miRNA-517) is yet unknown. Interestingly, however, two of the most up-regulated miRNAs measured by QRT-PCR were mir-372 and mir-373, which have recently been implicated in tumorigenesis [14].

Discussion

Since the initial description by Eberhart et al. [4], 14 cases of ETANTRs including our case have now been reported (Table 2). According to the statement by Dunham et al. [3], additional rare cases have likely been described in retrospect under different designations. According to the clinical data, ETANTRs are exclusively pediatric neoplasms with various localizations including cerebral hemispheres, cerebellum, and brainstem. Prognosis is regarded as extremely poor; however, one case with an event-free survival up to 34 months after intensive courses of hyper-fractionated radiotherapy and polychemotherapy has been documented [5]. In the case presented here, a cerebellar tumor in a 2-year-old child was subtotally removed, and high-dose chemotherapy followed by irradiation and maintenance chemotherapy resulted in 17 months progression-free survival.

Histopathologically, ETANTRs have a typical biphasic appearance. Usually ependymoblastoma-like rosettes and clusters of primitive neuroepithelial cells are embedded in areas of abundant neuropil. The present case showed predominately neuronal differentiation in both tumor components. Nevertheless, neuronal differentiation was more prominent in the neuropil-like matrix, whereas the primitive cells were intensively positive for vimentin.

Ultrastructural studies of several ETANTR cases describe patterns characteristic for neuronal (processes with numerous microtubules and neurosecretory granules) and ependymal (true rosettes with zonula adherences and basal bodies) cell differentiation. Cytogenetic findings were presented in two studies only. Fuller et al. [5] applied FISH analysis in two cases and described chromosome 17 abnormalities [including i(17q) in both tumors]. *MYC/MYCN* amplification as well as deletion of the *SMARCB1* locus was excluded. In contrast, Dunham et al. [3] studied one tumor and revealed normal DNA copy-numbers for the *MYC* and *MYCN* loci, and for chromosome 17.

In the present study, we performed genome-wide analysis of the ETANTR by using array-CGH with an average resolution of 0.5 Mb. Among the large-scale aberrations, there were trisomies of chromosomes 2 and 19 with a high-level amplicon at 19q13.42 spanning 0.89 Mb and covering numerous genes involved in carcinogenesis. We validated gains of chromosomes 2 and 19 applying FISH with corresponding probes. Besides, we found a few small regions of copy-number aberrations harboring potent oncogenes and tumor suppressor genes, although their biologic relevance for the pathogenesis of ETANTR requires further investigation.

Amplifications on 19q have been described in various human cancers, but in all these cases, more proximal parts of the chromosome arm (e.g., 19q12–13.3) were affected targeting well-established oncogenes (e.g., *CCNE* and *AKT2*). To our knowledge, this is the first description of a genomic amplification at 19q13.42. This region harbors 25 genes encoding a cluster of miRNAs. MicroRNAs have been implicated in different biological processes including human cancer. Various miRNAs were found to be involved in the pathogenesis of lung cancer, breast cancer, and lymphomas where they cooperate with oncogenes in cell transformation. Among the miRNAs located within the amplified region at 19q13.42, miRNA-372 and miRNA-373 have been recently identified as potent oncogenes in development of germ cell tumors by numbing the p53 pathway [14]. We performed miRNA expression profiling using a microarray covering most of the known human miRNAs, and found that expression of most of the miRNAs located within the miRNA cluster at 19q13.42 was highly upregulated in comparison with normal cerebellum, in which, we found virtually no expression of these miRNAs. The upregulation of selected miRNAs was confirmed by QRT-PCR. Expression of miRNA-372 and miRNA-373 was upregulated in the tumor by more than 30-fold in comparison with

normal cerebellum. These findings suggested a role of the miRNA cluster at 19q13.4 in the molecular pathogenesis of ETANTR.

The distinct nosologic position of ETANTR is still unclear. Clearly, ETANTR is an embryonal neoplasm that shows a wide spectrum of neuronal differentiation and additional features of ependymal differentiation. Eberhart et al. considered ETANTR to be a unique tumor entity that appears to be distinct from other forms of embryonal CNS tumors. In contrast, La Spina et al. suggested that ETANTR overlaps with other PNETs, including medulloblastomas with neuronal differentiation.

We compared the results of the current study with the results of previously performed array-CGH analyses of 100 medulloblastomas, 10 supratentorial PNETs, 12 AT/RTs, and 70 ependymomas applying the same microarray platform. Consequently, we found that the amplification on 19q13.42 has not been identified in any of these tumors indicating a specific aberration in ETANTR. Moreover, CGH analysis of four ependymoblastomas did not reveal aberrations on chromosome 19, although three of these tumors showed complete gains of chromosome 2 [11]. These findings allow us to hypothesize a unique nosologic position of ETANTR. Nevertheless, taking into account the rarity of these tumors, further molecular investigations will be necessary to finally answer this question. Such genome-wide screening analyses will be an important line of future research to identify the cell of origin of this infrequent tumor.

Acknowledgments We gratefully thank Andrea Wittmann for excellent technical assistance. This study was supported by a grant from the Landesstiftung Baden-Württemberg to SP ("Eliteprogramm für Postdoktoranden") and the NGFNplus Program of the BMBF (BTN 01GS0883).

References

1. Bubendorf L, Kononen J, Koivisto P, Schraml P, Moch H, Gasser TC, Willi N, Mihatsch MJ, Sauter G, Kallioniemi O-P (1999) Survey of gene amplifications during prostate cancer progression by high-throughput fluorescence in situ hybridization on tissue microarrays. Cancer Res 59(4):803–806
2. Castoldi M, Schmidt S, Benes V, Hentze MW, Muckenthaler MU (2008) miChip: an array-based method for microRNA expression profiling using locked nucleic acid capture probes. Nat Protoc 3(2):321–329
3. Dunham C, Sugo E, Tobias V, Wills E, Perry A (2007) Embryonal tumor with abundant neuropil and true rosettes (ETANTR): report of a case with prominent neurocytic differentiation. J Neurooncol 84(1):91–98
4. Eberhart C, Brat D, Cohen K, Burger P (2000) Pediatric neuroblastic brain tumors containing abundant neuropil and true rosettes. Pediatr Dev Pathol 3(4):346–352
5. Fuller C, Fouladi M, Gajjar A, Dalton J, Sanford R, Helton K (2006) Chromosome 17 abnormalities in pediatric neuroblastic tumor with abundant neuropil and true rosettes. Am J Clin Pathol 126(2):277–283
6. La Spina M, Pizzolitto S, Skrap M, Nocerino A, Russo G, Di Cataldo A, Perilongo G (2006) Embryonal tumor with abundant neuropil and true rosettes. A new entity or only variations of a parent neoplasms (PNETs)? This is the dilemma. J Neurooncol 78(3):317–320
7. Lichter P, Cremer T, Borden J, Manuelidis L, Ward D (1988) Delineation of individual human chromosomes in metaphase and interphase cells by in situ suppression hybridization using recombinant DNA libraries. Hum Genet 80(3):224–234
8. Louis D, Ohgaki H, Wiestler O, Cavenee W, Burger P, Jouvet A, Scheithauer B, Kleihues P (2007) The 2007 WHO classification of tumours of the central nervous system. Acta Neuropathol 114(2):97–109
9. Mendrzyk F, Radlwimmer B, Joos S, Kokocinski F, Benner A, Stange DE, Neben K, Fiegler H, Carter NP, Reifenberger G et al (2005) Genomic and protein expression profiling identifies CDK6 as novel independent prognostic marker in medulloblastoma. J Clin Oncol 23(34):8853–8862
10. Pfaffl MW (2001) A new mathematical model for relative quantification in real-time RT-PCR. Nucleic Acids Res 29(9):e45
11. Rickert C, Hasselblatt M (2006) Cytogenetic features of ependymoblastomas. Acta Neuropathol 111(6):559–562
12. Solinas-Toldo S, Lampel S, Stilgenbauer S, Nickolenko J, Benner A, Döhner H, Cremer T, Lichter P (1997) Matrix-based comparative genomic hybridization: biochips to screen for genomic imbalances. Genes Chromosomes Cancer 20(4):399–407
13. van den Boom J, Wolter M, Kuick R, Misek DE, Youkilis AS, Wechsler DS, Sommer C, Reifenberger G, Hanash SM (2003) Characterization of gene expression profiles associated with glioma progression using oligonucleotide-based microarray analysis and real-time reverse transcription-polymerase chain reaction. Am J Pathol 163(3):1033–1043
14. Voorhoeve PM, le Sage C, Schrier M, Gillis AJM, Stoop H, Nagel R, Liu Y-P, van Duijse J, Drost J, Griekspoor A et al (2006) A genetic screen implicates miRNA-372 and miRNA-373 as oncogenes in testicular germ cell tumors. Cell 124(6):1169–1181
15. Zielinski B, Gratias S, Toedt G, Mendrzyk F, Stange D, Radlwimmer B, Lohmann D, Lichter P (2005) Detection of chromosomal imbalances in retinoblastoma by matrix-based comparative genomic hybridization. Genes Chromosomes Cancer 43(3):294–301